Structural Chemistry
https://doi.org/10.1007/s11224-018-1180-7

ORIGINAL RESEARCH

DFT study of arsine (AsH_3) gas adsorption on pristine, Stone-Wales-defected, and Fe-doped single-walled carbon nanotubes

Javad Arasteh[1] · Mohamad Naseh[1]

Received: 11 July 2018 / Accepted: 21 August 2018

Abstract
To find the possible way of adsorption and detecting the toxic gas of AsH_3, we have studied the interactions between AsH_3 molecule and modified (5,5) single-walled carbon nanotubes by using the method of density functional theory (DFT). The interaction distances, adsorption energies, and geometry and electronic changes of structures were investigated to explore the sensitivity of variety of models of single-walled carbon nanotubes (SWCNTs) with Fe doping, Stone-Wales defects, and a combination of them toward AsH_3 molecule. From calculated results, it was found that AsH_3 molecule was more likely to be absorbed on Fe-doped CNTs with relatively higher adsorption energy and higher charge transfer and shorter interaction distance compared with that on the pristine and defected SWCNTs.

Keywords SWCNT · Adsorption · Stone-Wales defect · Doping · HOMO-LUMO gap

Introduction

Arsine (AsH_3) is a colorless toxic gas with mild garlic-like odor and slightly soluble in water that used in semiconductor industry [1, 2]. If small amount of AsH_3 was ingested into human body, it can trigger serious health problem such as disease so called arsenicosis [3–10]. Due to very strong toxicity of arsine, recently, its threshold limit value (TLV) is reduced to 5 ppb time-weighted average (TWA) [11]. So it is necessary to have continuous monitoring of this highly toxic gas in industrial buildings.

Carbon nanotubes (CNTs) have attracted considerable interest in light of their wide potential window in chemical properties and applications. Carbon nanotubes have strong abilities of adsorption and desorption for toxic gas molecules. It becomes potential resource for toxic gas detecting with changing the electrical conductivity of these materials upon presence and adsorption of these molecules in gaseous form. Meanwhile, the sensitivity of pure carbon nanotubes is only restricted to small range of gases.

✉ Mohamad Naseh
mohamadnaseh@yahoo.com

[1] Department of Chemistry, Dezful Branch, Islamic Azad University, Dezful, Iran

Doping some other atoms on the carbon nanotubes is an effective method for improving the gas-sensing properties of these materials [12–26]. By doping, more centers for gas interaction on the carbon nanotube surface are generated. By this strategy (doping), there is a potential possibility of carbon nanotubes serving as a chemical sensor for large variety of molecules such as poisonous gases [27–35]. Arsine adsorptions on the surface of graphene such as gold-modified reduced graphene oxide [1] and Sc-, Ti-, V-, and Cr-doped single-walled carbon nanotubes [14] were investigated and reported. Kunaseth et al. [36] used density functional theory (DFT) method to study arsine gas adsorption on palladium-doped graphene.

Another effective way to increase the sensitivity of CNTs to the molecules is making defects on the tubes. Previous experimental and theoretical studies showed that the existence of defects, such as vacancies [37], ad-dimer defect [38], Stone-Wales defect [39], and inverse Stone-Wales defect [40], in the structure of carbon nanomaterials can make change on the electronic [41, 42] and mechanical properties [43]. Zanolli et al. pointed out that defected CNTs could be used as a sensor for small molecules such as NO_2, NH_3, H_2O, and CO_2 [44]. Horner and co-workers found that SWCNTs with ad-dimer defects are chemically more reactive than perfect tube walls [45]. Roh et al. investigated the interaction of alkanethiol molecules and CNTs with Stone-Wales defect and found that these sites on the nanotube surface are active [46].

Published online: 30 August 2018

Dinadayalane et al. reported that 5775-Stone-Wales (SW)-defected CNTs are more sensitive for detecting methylene than perfect nanotubes [47].

In this work, we explore the sensitivity and adsorption behavior of pristine, Stone-Wales-defected, and Fe-doped CNTs to arsine toxic gas by means of DFT calculations.

Computational method

In order to examine the adsorption behavior of arsine gas molecule on pristine, Stone-Wales-defected, Fe-doped SWCNTs and a combination of them comprehensively, we selected (5,5) armchair semiconductor carbon nanotube which has 70 carbon atoms and 20 hydrogen atoms as the basic calculation model (see Fig. 1). The length of the nanotube is 7.34 Å, the diameter of it is 6.99 Å, and the average C–C bond length is 1.42 Å. Fe transition metal atom was doped onto the (5,5) SWCNT by replacing one carbon atom of the (5,5) SWCNT with Fe atom. Structure, electronic properties, charge transfer, and adsorption energy were performed on AsH_3 adsorption on pristine, Fe-doped, and defected (5,5) single-walled carbon nanotubes. Electronic properties of the arsine adsorbed on the CNTs were compared with each other by using GaussSum 2.2.5 program [48] and plotting electronic density of state (DOS) for all structures. Nanotube and arsine were placed together in an input file to be optimized in presence of each other. All the calculations were completed with the Gaussian 09 software [49] using the density functional theory (DFT) and were performed using the B3LYP [50, 51] method and Los Alamos LanL2DZ split-valence basis set [52–54].

To evaluate the interaction between the AsH_3 gas and pristine SWCNT (PS-SWCNT), Fe-doped SWCNT (Fe-SWCNT), 5775-Stone-Wales-defected SWCNT (5775-SWCNT), and 7557-Stone-Wales-defected SWCNT (7557-SWCNT), their adsorption energies (E_{ads}) were calculated by Eqs. (1), (2), (3), and (4), respectively.

$$E_{ads} = E\,(AsH_3/PS{-}SWCNT){-}E\,(PS{-}SWCNT){-}E\,(AsH_3) \quad (1)$$

$$E_{ads} = E\,(AsH_3/Fe{-}SWCNT){-}E\,(Fe{-}SWCNT){-}E\,(AsH_3) \quad (2)$$

$$E_{ads} = E\,(AsH_3/5775{-}SWCNT){-}E\,(5775{-}SWCNT){-}E\,(AsH_3) \quad (3)$$

$$E_{ads} = E\,(AsH_3/7557{-}SWCNT){-}E\,(7557{-}SWCNT){-}E\,(AsH_3) \quad (4)$$

An exothermic or endothermic process has a negative or positive value for E_{ads}, respectively. According to the obtained

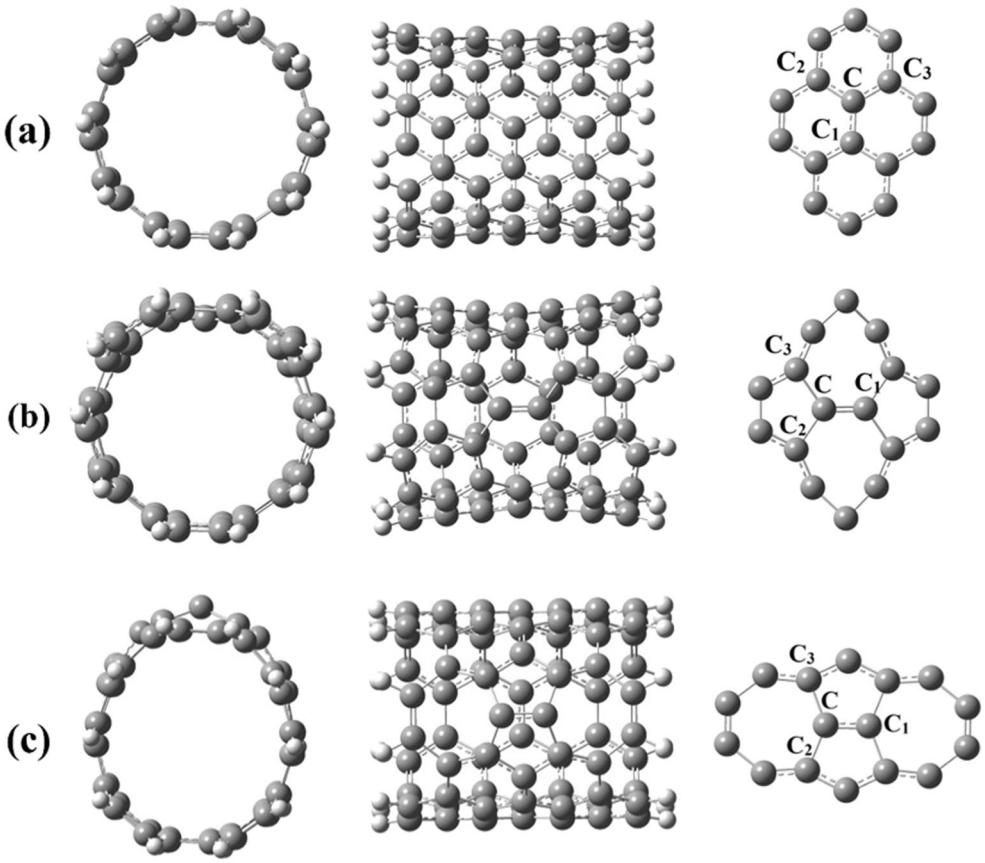

Fig. 1 The B3LYP/LanL2DZ optimized structures of **a** PS-SWCNT, **b** 5775-SWCNT, and **c** 7557-SWCNT

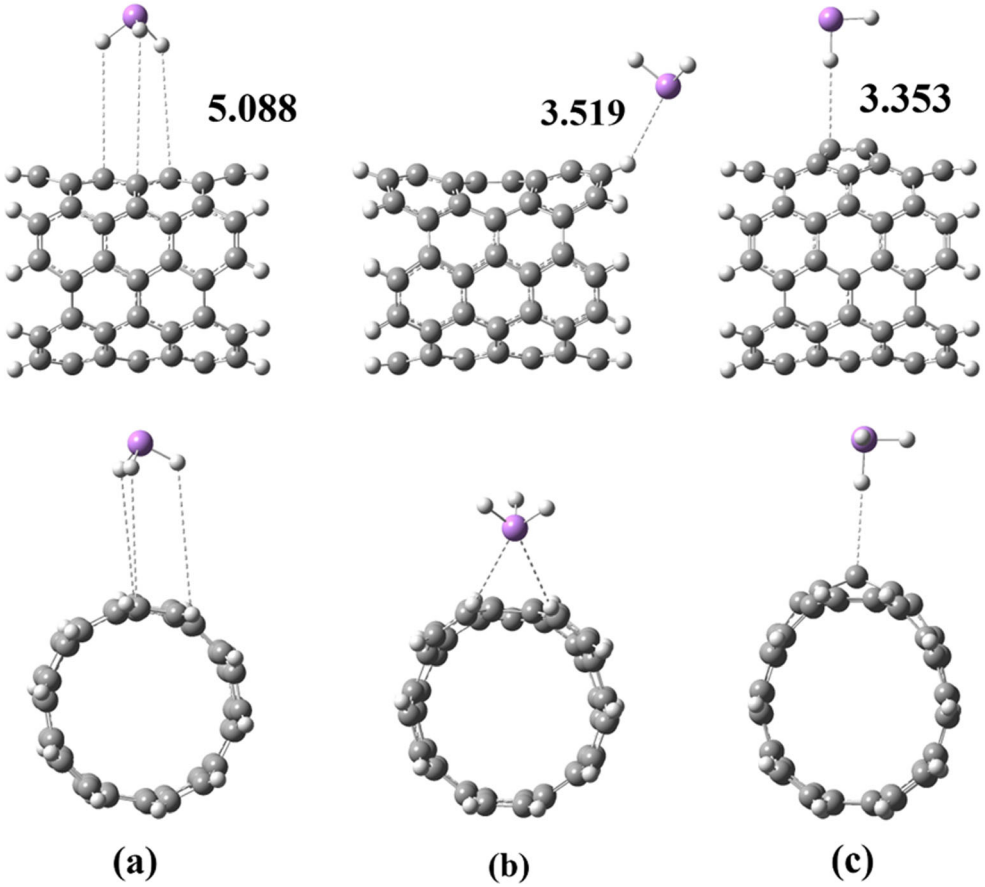

Fig. 2 The B3LYP/LanL2DZ optimized structures of the AsH_3 molecule adsorption configurations of **a** AsH_3/PS-SWCNT, **b** AsH_3/5775-SWCNT, and **c** AsH_3/7557-SWCNT. Top and bottom are side and front views of tubes. Bond distances are in Å

Table 1 Selected geometrical parameters of the pristine and Stone-Wales-defected SWCNTs, their Fe-doped structures, and their AsH_3 adsorptions, computed at the B3LYP/LanL2DZ level

Species	Bond length (Å)			Binding distance (Å)	Bond angle (°)		
	C_1–M[a,b]	C_2–M[a,b]	C_3–M[a,b]		C_1–M–C_2	C_2–M–C_3	C_3–M–C_1
PS-SWCNT							
PS-SWCNT	1.417	1.441	1.441	–	118.596	120.233	118.596
Fe-PS-SWCNT	1.880	1.785	1.785	–	92.018	97.310	92.018
AsH_3/PS-SWCNT	1.418	1.441	1.441	5.088	119.333	119.820	117.930
AsH_3/Fe-PS-SWCNT	1.824	1.793	1.793	2.529	93.221	99.077	93.224
5775-SWCNT							
5775-SWCNT	1.352	1.467	1.467	–	126.575	106.834	126.575
Fe-5775-SWCNT	1.737	1.794	1.794	–	100.835	87.885	100.835
AsH_3/5775-SWCNT	1.352	1.467	1.467	3.519	126.577	106.831	126.576
AsH_3/Fe-5775-SWCNT	1.692	1.836	1.846	2.529	97.168	89.217	98.229
7557-SWCNT							
7557-SWCNT	1.405	1.467	1.467	–	108.882	120.656	108.883
Fe-7557-SWCNT	1.781	1.884	1.884	–	85.170	91.536	85.170
AsH_3/7557-SWCNT	1.406	1.467	1.467	3.353	108.857	120.750	108.865
AsH_3/Fe-7557-SWCNT	1.783	1.906	1.906	2.496	83.326	87.522	84.725

[a] C_1, C_2, and C_3 are atoms on the SWCNTs which are defined in Fig. 1

[b] M is C atom for without Fe doping species and Fe metal which is doped on SWCNT species labeled in Figs. 1 and 4, respectively

Table 2 The adsorption energy (E_{ads}), the distance between AsH_3 and nanotube (D), and the charge transfer from AsH_3 molecule to tube

Configuration	E_{ads} (kcal/mol)	D (Å)	Q (e)
AsH_3/PS-SWCNT	− 0.27	5.088	0
AsH_3/5775-SWCNT	− 0.79	3.519	+ 0.002
AsH_3/7557-SWCNT	− 0.35	3.353	+ 0.040

results, exothermic process with negative value for adsorption energy represents stronger interaction between AsH_3 and single-walled carbon nanotubes.

Table 3 The highest occupied molecular orbital energies (E_{HOMO}), the lowest unoccupied molecular orbital energies (E_{LUMO}), and HOMO-LUMO energy gap (HLG) of pristine (PS-SWCNT) and Stone-Wales-defected SWCNT (5775-SWCNT and 7557-SWCNT) and their AsH_3 adsorption structures

Species	E_{LUMO}	E_{HOMO}	HLG
PS-SWCNT	− 2.67	− 4.88	2.21
AsH_3/PS-SWCNT	− 2.68	− 4.90	2.22
5775-SWCNT	− 2.85	− 4.91	2.06
AsH_3/5775-SWCNT	− 2.72	− 4.98	2.26
7557-SWCNT	− 2.95	− 5.16	2.21
AsH_3/7557-SWCNT	− 2.98	− 5.18	2.20

Results and discussion

Adsorption of arsine on pristine and defected CNTs

We first studied the adsorption of AsH_3 molecule on the pristine and defected (5,5) CNT without Fe doping. The optimized structure of pristine and Stone-Wales-defected (5775-SWCNT and 7557-SWCNT) (5,5) CNT was displayed in Fig. 2, and bond lengths and bond angles of the structures are listed in Table 1. The adsorptions of arsine gas molecule on the pristine CNT are not affected by the C–C_1, C–C_2, and C–C_3 bond lengths. The adsorption energies (E_{ads}), shortest distance between the As atom of arsine and the nearest carbon atom (D), and charge transfer from AsH_3 to CNT were all presented in Table 2. From data of Table 2, it indicates that the shortest distance between As atom and CNT is 3.353 Å from AsH_3/7557-SWCNT configuration.

The adsorption energy and charge transfer are − 0.35 kcal/mol and 0.040 e, respectively. These results showed that the interaction between AsH_3 molecule and 7557-SWCNT was weak electrostatic interaction. Like this, the interaction distance between gas molecule and substrate was relatively long; the electrostatic interaction was weak and the charge transfer is small, so we could say the adsorption between gas and CNT would be physical adsorption. The adsorption energy, distance between As and CNT, and charge transfer for interaction between arsine and perfect site CNT (AsH_3/PS-SWCNT) are − 0.27 kcal/mol, 5.088 Å, and zero electron, respectively, and these parameters for interaction between As and 5775-defected CNT (AsH_3/5775-SWCNT) are − 0.79 kcal/mol, 3.519 Å, and 0.002 e, respectively. These parameters indicated that in two configurations of AsH_3/PS-SWCNT and AsH_3/5775-SWCNT, arsine molecule adsorbed on CNT was physical adsorption and the electrostatic interactions were weak.

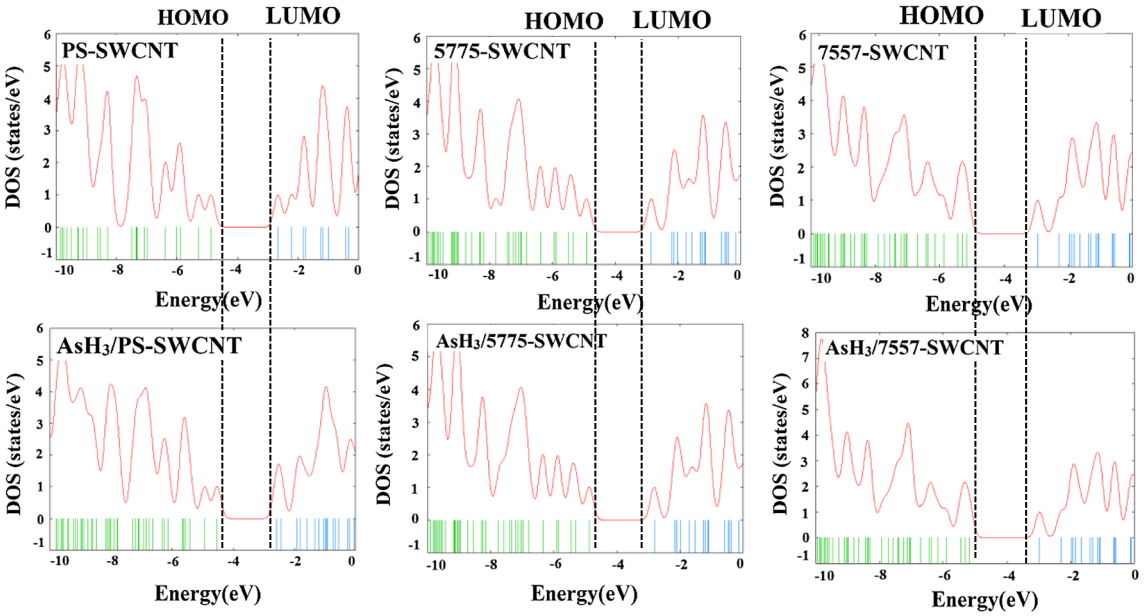

Fig. 3 The density of state plots of PS-SWCNT, AsH_3/PS-SWCNT, 5775-SWCNT, AsH_3/5775-SWCNT, 7557-SWCNT, and AsH_3/7557-SWCNT

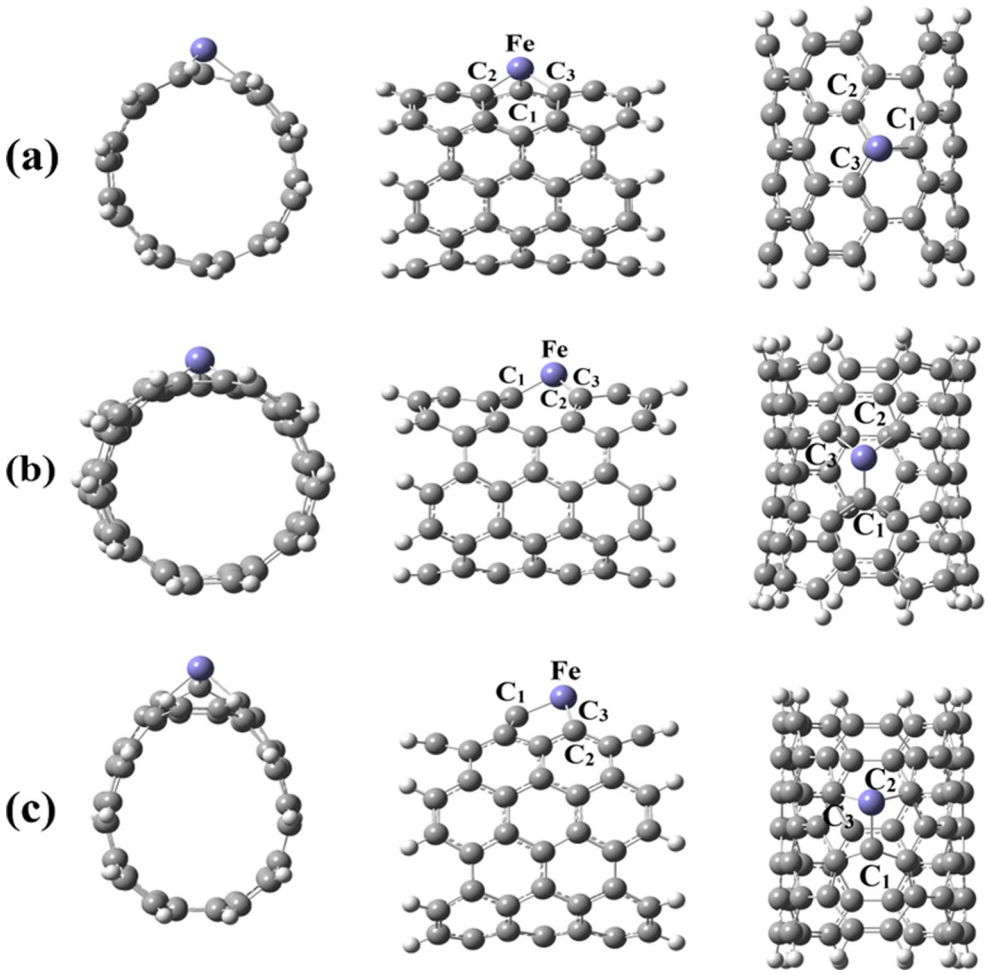

Fig. 4 The B3LYP/LanL2DZ optimized structures of the Fe-doped as **a** Fe-PS-SWCNT, **b** Fe-5775-SWCNT, and **c** Fe-7557-SWCNT. Right and left are side and front views of tubes

In order to deeply understand the effects of defects on AsH_3 adsorption on CNTs, the electronic properties of these systems were obtained and analyzed by density of states (DOS) plots. As shown in Fig. 3, the DOS of PS-SWCNT, AsH_3/PS-SWCNT, 5775-SWCNT, AsH_3/5775-SWCNT, 7557-SWCNT, and AsH_3/7557-SWCNT were depicted. Also, energies of HOMO, LUMO, and HOMO-LUMO gap (HLG) were all presented in Table 3. It was found that there was no significant change between the PS-SWCNT and AsH_3/PS-SWCNT, and PS-SWCNT after adsorption of AsH_3 still presented the characteristics of semiconductor. Also, for 7557-SWCNT and AsH_3/7557-SWCNT, the same results are obtained. From the calculated results of band gap energies, 5775-SWCNT was 2.06 eV before adsorbing AsH_3, which became 2.26 eV in AsH_3/5775-SWCNT configuration indicating that the 5775-SWCNT was more sensitive to detect AsH_3 molecule by decreasing electrical conductivity.

Table 4 The adsorption energy (E_{ads}), the distance between AsH_3 and nanotube (D), and the charge transfer from AsH_3 molecule to tube

Configuration	E_{ads} (kcal/mol)	D (Å)	Q (e)
AsH_3/Fe-PS-SWCNT	− 57.34	2.529	0.142
AsH_3/Fe-5775-SWCNT	− 50.79	2.529	0.138
AsH_3/Fe-7557-SWCNT	− 16.00	2.496	0.317

Adsorption of AsH_3 on pristine and defected CNTs with Fe-doped

In this section, we investigated the adsorption of AsH_3 molecule on Fe-doped and Fe-doped defected CNTs. We used the Fe atom to replace the C atom of CNT, and structures of Fe-PS-SWCNT, Fe-5775-SWCNT, and Fe-7557-SWCNT were made. When doping Fe atom on the structures, the geometry of structures was dramatically changed. By geometry optimization, the Fe atom located out of the tube wall and there was an embossment at the Fe-doped site, because of the bigger radius of Fe atom (Fig. 4). Taking Fe-5775-SWCNT as example for analysis, we found that the calculated bond lengths of C_1–Fe, C_2–Fe, and C_3–Fe were 1.737, 1.794, and 1.794 Å which were longer than those of C_1–C, C_2–C, and C_3–C with the values of 1.417, 1.441, and 1.441 Å in 5775-SWCNT configuration, respectively.

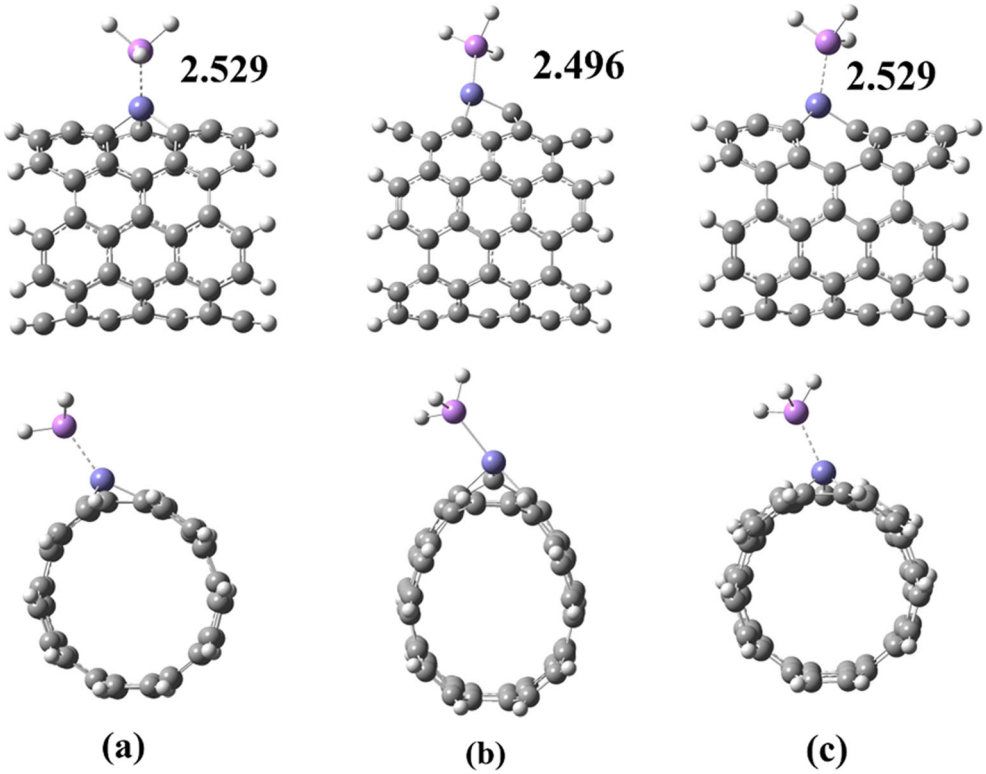

Fig. 5 The B3LYP/LanL2DZ optimized structures of the AsH_3 molecule adsorption configurations of **a** AsH_3/Fe-PS-SWCNT, **b** AsH_3/Fe-5775-SWCNT, and **c** AsH_3/Fe-7557-SWCNT. Top and bottom are side and front views of tubes. Bond distances are in Å

The corresponding adsorption energy, interaction distance between AsH_3 and Fe atom, and charge transfer were listed in Table 4. In general, the values of E_{ads} of Fe-doped structures were all larger than those of CNT without Fe doping, which was an evidence that the Fe dopant significantly enhanced the adsorption process. As shown in Table 4, the adsorption energy (E_{ads}) of the AsH_3/Fe-PS-SWCNT configuration was − 57.34 kcal/mol which was larger than that of AsH_3/PS-SWCNT (− 0.27 kcal/mol). Also for defected systems, AsH_3/Fe-5775-SWCNT and AsH_3/Fe-7557-SWCNT, the E_{ads} were − 50.79 kcal/mol and − 16.00 kcal/mol which were larger than those of AsH_3/5775-SWCNT (− 0.79 kcal/mol) and AsH_3/7557-SWCNT (− 0.35 kcal/mol), respectively.

The adsorption distances (Fig. 5) of AsH_3/Fe-PS-SWCNT, AsH_3/Fe-5775-SWCNT, and AsH_3/Fe-7557-SWCNT configurations (2.529 Å, 2.529 Å, and 2.496 Å) were also smaller

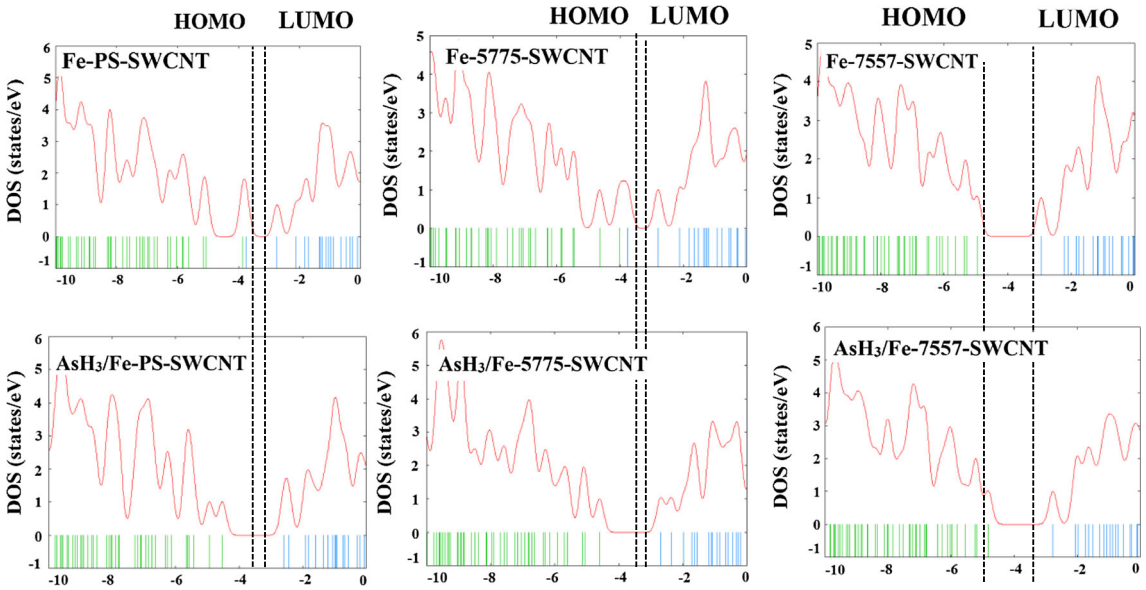

Fig. 6 The density of state plots of Fe-PS-SWCNT, AsH_3/Fe-PS-SWCNT, Fe-5775-SWCNT, AsH_3/Fe-5775-SWCNT, Fe-7557-SWCNT, and AsH_3/Fe-7557-SWCNT

Table 5 The highest occupied molecular orbital energies (E_{HOMO}), the lowest unoccupied molecular orbital energies (E_{LUMO}), and HOMO-LUMO energy gap (HLG) of Fe-doped pristine (Fe-PS-SWCNT) and Fe-doped Stone-Wales-defected SWCNT (Fe-5775-SWCNT and Fe-7557-SWCNT) and their AsH_3 adsorption structures

Species	E_{LUMO}	E_{HOMO}	HLG
Fe-PS-SWCNT	− 3.76	− 3.87	0.11
AsH_3/Fe-PS-SWCNT	− 2.58	− 4.53	1.95
Fe-5775-SWCNT	− 3.76	− 4.01	0.25
AsH_3/Fe-5775-SWCNT	− 2.69	− 4.60	1.91
Fe-7557-SWCNT	− 2.95	− 4.96	2.01
AsH_3/Fe-7557-SWCNT	− 2.77	− 4.83	2.06

than those of AsH_3/PS-SWCNT, AsH_3/5775-SWCNT, and AsH_3/7557-SWCNT (5.088 Å, 3.519 Å, and 3.353 Å, respectively). The larger adsorption energies (E_{ads}) and smaller interaction distances (D) indicate that the presence of Fe dopant improved the activity of PS-SWCNT and defected SWCNTs.

For further study, the enhancement of the Fe doping on the AsH_3 adsorption, density of states (DOS) of systems, and charge transfer that changed between AsH_3 and substrate had been calculated. Figure 6 showed the DOS of systems around the Fermi level. Also, energies of HOMO, LUMO, and HOMO-LUMO gap (HLG) were all presented in Table 5. From the calculated results of HOMO-LUMO gap energies, Fe-PS-SWCNT and Fe-5775-SWCNT systems were 0.11 eV and 0.25 eV before adsorbing AsH_3 which became 1.95 eV and 1.91 eV in AsH_3/Fe-PS-SWCNT and AsH_3/Fe-5775-SWCNT, respectively, while HOMO-LUMO gap energy of Fe-7557-SWCNT was 2.01 eV before adsorbing AsH_3, which became 2.06 eV in AsH_3/Fe-7557-SWCNT. So, it was resulted that conductivities of Fe-PS-SWCNT and Fe-5775-SWCNT were decreased during adsorption but there was no significant change between HLG of Fe-7557-SWCNT and AsH_3/Fe-7557-SWCNT after adsorption of AsH_3.

Upon the adsorption process, the HOMO and LUMO levels are significantly changed. For example, for adsorption of AsH_3 on Fe-PS-SWCNT configuration, the HOMO is stabilized from − 3.87 to − 4.53 eV and the LUMO is destabilized from − 3.76 to − 2.58 eV (Table 5). The shapes of the HOMO and LUMO are changed in accordance with the energy change. As shown in Fig. 7, the HOMO level of structures is shifted on Fe atom, near rings, and AsH_3 molecule and the LUMO is generally distributed on all atoms of tube. The change of the energy of the LUMO level is much more than that of the HOMO level for AsH_3/Fe-PS-SWCNT and AsH_3/Fe-5775-SWCNT, and thus, the HLG is significantly changed by about 1672% and 664%, respectively.

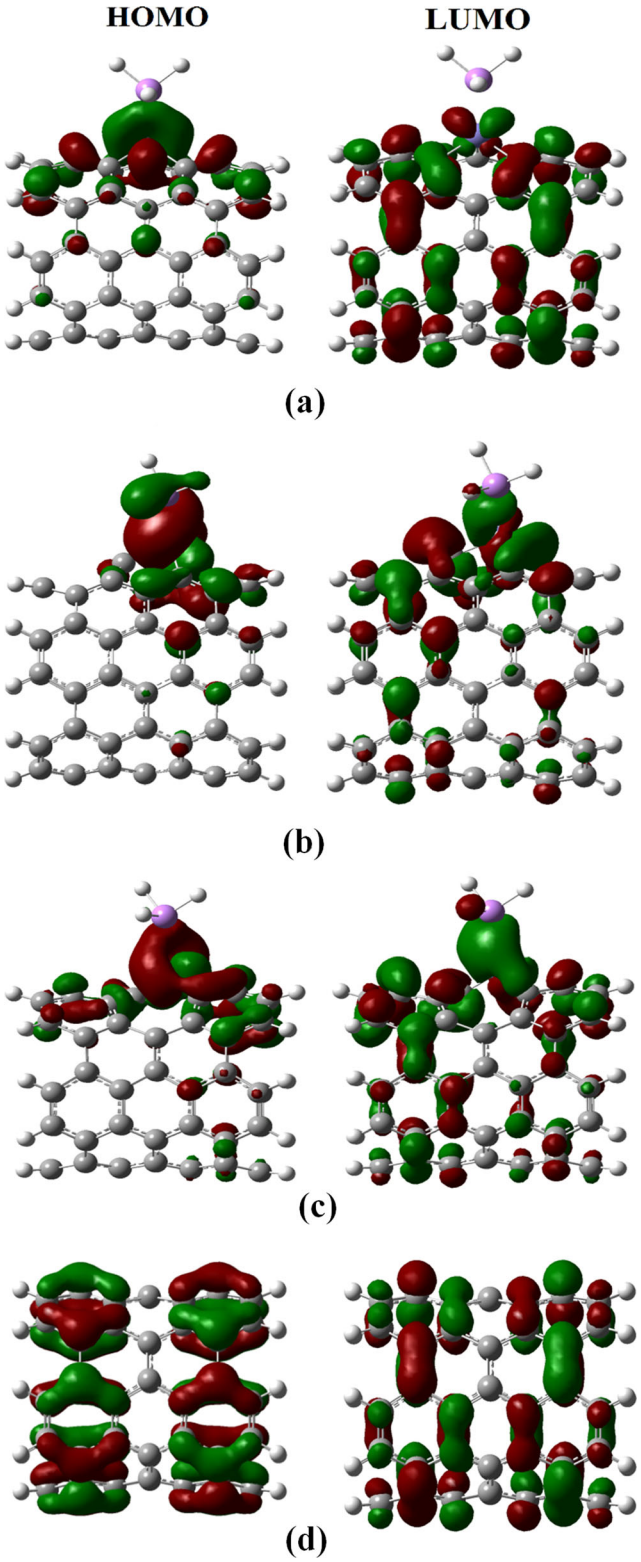

Fig. 7 The plots of HOMOs (left) and LUMOs (right) of **a** AsH_3/Fe-PS-SWCNT, **b** AsH_3/Fe-5775-SWCNT, and **c** AsH_3/Fe-7557-SWCNT **d** pristine SWCNT, computed at the B3LYP/LanL2DZ level

All calculations of adsorption energies (E_{ads}) and electronic properties (HLG) suggest that the interactions between the AsH_3 molecule and the Fe-doped structures are stronger than the interactions between the AsH_3 molecule and the undoped structures. So, the Fe-PS-SWCNT and Fe-5775-SWCNT systems had the potential capacities to develop sensors for AsH_3 toxic gas detecting.

Conclusions

Using the density functional theory (DFT) method, we explored that possibility of Stone-Wales-defected carbon nanotube (CNT) doped with Fe as a potential efficient sensor device for the arsine (AsH_3) gas molecule. The results indicated that the presence of Stone-Wales defect and the dopant increased the sensitivity of CNT substrate toward the arsine molecule. Furthermore, the band gap was increased during the adsorption of arsine molecule on the Fe-doped and Stone-Wales-defected Fe-doped CNTs which could be seen as an electric signal to detect the arsine molecule. The findings of the present study will lay a road in the development of chemical nanosensor based on CNT material for arsine detection.

Acknowledgments The authors would like to thank the Islamic Azad University, Dezful Branch, for computational resources.

Funding information This work was financially supported by the Islamic Azad University, Dezful Branch.

Compliance with ethical standards

Conflict of interest The authors declare that they have no conflict of interest.

References

1. Furue R, Koveke EP, Sugimoto S, Shudo Y, Hayami S, Ohira S-I, Toda K (2017) Arsine gas sensor based on gold-modified reduced graphene oxide. Sensors Actuators B Chem 240:657–663. https://doi.org/10.1016/j.snb.2016.08.131
2. Pakulska D, Czerczak S (2014) Arsine A2 - Wexler, Philip. Encyclopedia of toxicology3rd edn. Academic Press, Oxford, pp 313–316. https://doi.org/10.1016/B978-0-12-386454-3.00005-1
3. Steinmaus CM, Ferreccio C, Romo JA, Yuan Y, Cortes S, Marshall G, Moore LE, Balmes JR, Liaw J, Golden T (2013) Drinking water arsenic in northern Chile: high cancer risks 40 years after exposure cessation. Cancer Epidemiology and Prevention Biomarkers:cebp 1190.2012
4. Saha J, Dikshit A, Bandyopadhyay M, Saha K (1999) A review of arsenic poisoning and its effects on human health. Crit Rev Environ Sci Technol 29(3):281–313
5. Meliker JR, Wahl RL, Cameron LL, Nriagu JO (2007) Arsenic in drinking water and cerebrovascular disease, diabetes mellitus, and kidney disease in Michigan: a standardized mortality ratio analysis. Environ Health 6(1):4
6. Mazumder DNG, Haque R, Ghosh N, De BK, Santra A, Chakraborti D, Smith AH (2000) Arsenic in drinking water and the prevalence of respiratory effects in West Bengal, India. Int J Epidemiol 29(6):1047–1052
7. Hughes MF, Beck BD, Chen Y, Lewis AS, Thomas DJ (2011) Arsenic exposure and toxicology: a historical perspective. Toxicol Sci 123(2):305–332
8. Chung JS, Kalman DA, Moore LE, Kosnett MJ, Arroyo AP, Beeris M, Mazumder DG, Hernandez AL, Smith AH (2002) Family correlations of arsenic methylation patterns in children and parents exposed to high concentrations of arsenic in drinking water. Environ Health Perspect 110(7):729
9. Chen Y, Parvez F, Gamble M, Islam T, Ahmed A, Argos M, Graziano JH, Ahsan H (2009) Arsenic exposure at low-to-moderate levels and skin lesions, arsenic metabolism, neurological functions, and biomarkers for respiratory and cardiovascular diseases: review of recent findings from the Health Effects of Arsenic Longitudinal Study (HEALS) in Bangladesh. Toxicol Appl Pharmacol 239(2):184–192
10. Argos M, Parvez F, Chen Y, Hussain AI, Momotaj H, Howe GR, Graziano JH, Ahsan H (2007) Socioeconomic status and risk for arsenic-related skin lesions in Bangladesh. Am J Public Health 97(5):825–831
11. Tchounwou PB, Yedjou CG, Patlolla AK, Sutton DJ (2012) Heavy metals toxicity and the environment. EXS 101:133–164. https://doi.org/10.1007/978-3-7643-8340-4_6
12. Abdulla S, Mathew TL, Pullithadathil B (2015) Highly sensitive, room temperature gas sensor based on polyaniline-multiwalled carbon nanotubes (PANI/MWCNTs) nanocomposite for trace-level ammonia detection. Sensors Actuators B Chem 221:1523–1534. https://doi.org/10.1016/j.snb.2015.08.002
13. Azam MA, Alias FM, Tack LW, Seman RNAR, Taib MFM (2017) Electronic properties and gas adsorption behaviour of pristine, silicon-, and boron-doped (8, 0) single-walled carbon nanotube: a first principles study. J Mol Graph Model 75:85–93. https://doi.org/10.1016/j.jmgm.2017.05.003
14. Buasaeng P, Rakrai W, Wanno B, Tabtimsai C (2017) DFT investigation of NH3, PH3, and AsH3 adsorptions on Sc-, Ti-, V-, and Cr-doped single-walled carbon nanotubes. Appl Surf Sci 400:506–514. https://doi.org/10.1016/j.apsusc.2016.12.215
15. Chimowa G, Tshabalala ZP, Akande AA, Bepete G, Mwakikunga B, Ray SS, Benecha EM (2017) Improving methane gas sensing properties of multi-walled carbon nanotubes by vanadium oxide filling. Sensors Actuators B Chem 247:11–18. https://doi.org/10.1016/j.snb.2017.02.167
16. Dhall S, Sood K, Nathawat R (2017) Room temperature hydrogen gas sensors of functionalized carbon nanotubes based hybrid nanostructure: role of Pt sputtered nanoparticles. Int J Hydrog Energy 42(12):8392–8398. https://doi.org/10.1016/j.ijhydene.2017.02.005
17. Izakmehri Z, Ganji MD, Ardjmand M (2017) Adsorption of 2, 3, 7, 8-tetrachlorodibenzo-p-dioxin (TCDD) on pristine, defected and Al-doped carbon nanotube: a dispersion corrected DFT study. Vacuum 136:51–59. https://doi.org/10.1016/j.vacuum.2016.11.025
18. Khorram R, Raissi H, Morsali A (2017) Assessment of solvent effects on the interaction of Carmustine drug with the pristine and COOH-functionalized single-walled carbon nanotubes: a DFT perspective. J Mol Liq 240:87–97. https://doi.org/10.1016/j.molliq.2017.05.035
19. Kwon YJ, Na HG, Kang SY, Choi S-W, Kim SS, Kim HW (2016) Selective detection of low concentration toluene gas using Pt-decorated carbon nanotubes sensors. Sensors Actuators B Chem 227:157–168. https://doi.org/10.1016/j.snb.2015.12.024
20. Mittal M, Kumar A (2014) Carbon nanotube (CNT) gas sensors for emissions from fossil fuel burning. Sensors Actuators B Chem 203:349–362. https://doi.org/10.1016/j.snb.2014.05.080

21. Mollania F, Raissi H (2017) Evaluation of solvent and ion effects upon leflunomide adsorption characteristics on (6,0) zigzag single-walled carbon nanotube and immobilized dihydroorotate dehydrogenase activity: a computational DFT and experimental study. J Mol Liq 231:528–541. https://doi.org/10.1016/j.molliq.2017.02.010
22. Shahabi D, Tavakol H (2017) DFT, NBO and molecular docking studies of the adsorption of fluoxetine into and on the surface of simple and sulfur-doped carbon nanotubes. Appl Surf Sci 420:267–275. https://doi.org/10.1016/j.apsusc.2017.05.068
23. Saadat K, Tavakol H (2016) Study of noncovalent interactions of end-caped sulfur-doped carbon nanotubes using DFT, QTAIM, NBO and NCI calculations. Struct Chem 27(3):739–751. https://doi.org/10.1007/s11224-015-0616-6
24. Hamadanian M, Khoshnevisan B, Fotooh FK (2011) Density functional study of super cell N-doped (10,0) zigzag single-walled carbon nanotubes as CO sensor. Struct Chem 22(6):1205–1211. https://doi.org/10.1007/s11224-011-9814-z
25. Saikia N, Deka RC (2013) Density functional study on the adsorption of the drug isoniazid onto pristine and B-doped single wall carbon nanotubes. J Mol Model 19(1):215–226. https://doi.org/10.1007/s00894-012-1534-9
26. Bian R, Zhao J, Fu H (2013) Silicon–doping in carbon nanotubes: formation energies, electronic structures, and chemical reactivity. J Mol Model 19(4):1667–1675. https://doi.org/10.1007/s00894-012-1733-4
27. Azizi K, Karimpanah M (2013) Computational study of Al- or P-doped single-walled carbon nanotubes as NH3 and NO2 sensors. Appl Surf Sci 285:102–109. https://doi.org/10.1016/j.apsusc.2013.07.146
28. Jijun Z, Alper B, Jie H, Jian Ping L (2002) Gas molecule adsorption in carbon nanotubes and nanotube bundles. Nanotechnology 13(2):195–200
29. Park S, Park S, So H-M, Jeon E-K, Park D-W, Kim J-J, Kim BS, K-j K, Chang H, Lee J-O (2010) Computer-aided design and growth of single-walled carbon nanotubes on 4 in. wafers for electronic device applications. Carbon 48(8):2218–2224. https://doi.org/10.1016/j.carbon.2010.02.030
30. Peng S, Cho K (2003) Ab initio study of doped carbon nanotube sensors. Nano Lett 3(4):513–517. https://doi.org/10.1021/nl034064u
31. Tabtimsai C, Keawwangchai S, Wanno B, Ruangpornvisuti V (2012) Gas adsorption on the Zn–, Pd– and Os–doped armchair (5,5) single–walled carbon nanotubes. J Mol Model 18(1):351–358. https://doi.org/10.1007/s00894-011-1047-y
32. Yoosefian M, Barzgari Z, Yoosefian J (2014) Ab initio study of Pd-decorated single-walled carbon nanotube with C-vacancy as CO sensor. Struct Chem 25(1):9–19. https://doi.org/10.1007/s11224-013-0220-6
33. Yoosefian M, Raissi H, Mola A (2015) The hybrid of Pd and SWCNT (Pd loaded on SWCNT) as an efficient sensor for the formaldehyde molecule detection: a DFT study. Sensors Actuators B Chem 212:55–62. https://doi.org/10.1016/j.snb.2015.02.004
34. Zhou Q, Wang C, Fu Z, Zhang H, Tang Y (2014) Adsorption of formaldehyde molecule on Al-doped vacancy-defected single-walled carbon nanotubes: a theoretical study. Comput Mater Sci 82:337–344. https://doi.org/10.1016/j.commatsci.2013.09.046
35. Zhou X, Tian WQ, Wang X-L (2010) Adsorption sensitivity of Pd-doped SWCNTs to small gas molecules. Sensors Actuators B Chem 151(1):56–64. https://doi.org/10.1016/j.snb.2010.09.054
36. Kunaseth M, Mudchimo T, Namuangruk S, Kungwan N, Promarak V, Jungsuttiwong S (2016) A DFT study of arsine adsorption on palladium doped graphene: effects of palladium cluster size. Appl Surf Sci 367:552–558. https://doi.org/10.1016/j.apsusc.2016.01.139
37. Stankovich S, Dikin D, Dommett GHB, Kohlhaas KM, Zimney EJ, Stach EA, Piner RD, Nguyen ST, Ruoff RS (2006). Nature 442:282
38. Barbolina I, Novoselov K, Morozov S, Dubonos S, Missous M, Volkov A, Christian D, Grigorieva I, Geim A (2006) Submicron sensors of local electric field with single-electron resolution at room temperature. Appl Phys Lett 88(1):013901
39. Schedin F, Geim A, Morozov S, Hill E, Blake P, Katsnelson M, Novoselov K (2007) Detection of individual gas molecules adsorbed on graphene. Nat Mater 6(9):652
40. Di C, Wei D, Yu G, Liu Y, Guo Y, Zhu D (2008) Patterned graphene as source/drain electrodes for bottom-contact organic field-effect transistors. Adv Mater 20(17):3289–3293
41. Lee J, Ladd AJ (2005) Axial segregation of a settling suspension in a rotating cylinder. Phys Rev Lett 95(4):048001
42. Duplock EJ, Scheffler M, Lindan PJ (2004) Hallmark of perfect graphene. Phys Rev Lett 92(22):225502
43. Ribeiro FJ, Tangney P, Louie SG, Cohen ML (2005) Structural and electronic properties of carbon in hybrid diamond-graphite structures. Phys Rev B 72(21):214109
44. Zanolli Z, Charlier J-C (2009) Defective carbon nanotubes for single-molecule sensing. Phys Rev B 80(15):155447
45. Horner D, Redfern PC, Sternberg M, Zapol P, Curtiss LA (2007) Increased reactivity of single wall carbon nanotubes at carbon adimer defect sites. Chem Phys Lett 450(1–3):71–75
46. Poblenz C, Waltereit P, Rajan S, Heikman S, Mishra U, Speck J (2004) Effect of carbon doping on buffer leakage in AlGaN/GaN high electron mobility transistors. Journal of Vacuum Science & Technology B: Microelectronics and Nanometer Structures Processing, Measurement, and Phenomena 22(3):1145–1149
47. Dinadayalane T, Murray JS, Concha MC, Politzer P, Leszczynski J (2010) Reactivities of sites on (5, 5) single-walled carbon nanotubes with and without a Stone-Wales defect. J Chem Theory Comput 6(4):1351–1357
48. O'Boyle NM, Tenderholt AL, Langner KM (2008) cclib: a library for package-independent computational chemistry algorithms. J Comput Chem 29(5):839–845. https://doi.org/10.1002/jcc.20823
49. Frisch MJ, Trucks GW, Schlegel HB, Scuseria GE, Robb MA, Cheeseman JR, Scalmani G, Barone V, Mennucci B, Petersson GA, Nakatsuji H, Caricato M, Li X, Hratchian HP, Izmaylov AF, Bloino J, Zheng G, Sonnenberg JL, Hada M, Ehara M, Toyota K, Fukuda R, Hasegawa J, Ishida M, Nakajima T, Honda Y, Kitao O, Nakai H, Vreven T, Montgomery Jr JA, Peralta JE, Ogliaro F, Bearpark MJ, Heyd J, Brothers EN, Kudin KN, Staroverov VN, Kobayashi R, Normand J, Raghavachari K, Rendell AP, Burant JC, Iyengar SS, Tomasi J, Cossi M, Rega N, Millam NJ, Klene M, Knox JE, Cross JB, Bakken V, Adamo C, Jaramillo J, Gomperts R, Stratmann RE, Yazyev O, Austin AJ, Cammi R, Pomelli C, Ochterski JW, Martin RL, Morokuma K, Zakrzewski VG, Voth GA, Salvador P, Dannenberg JJ, Dapprich S, Daniels AD, Farkas Ö, Foresman JB, Ortiz JV, Cioslowski J, Fox DJ (2009) Gaussian 09. Gaussian, Inc., Wallingford
50. Becke AD (1993) Becke's three parameter hybrid method using the LYP correlation functional. J Chem Phys 98:5648–5652
51. Lee C, Yang W, Parr RG (1988) Development of the Colle-Salvetti correlation-energy formula into a functional of the electron density. Phys Rev B 37(2):785–789
52. Hay PJ, Wadt WR (1985) Ab initio effective core potentials for molecular calculations. Potentials for K to Au including the outermost core orbitals. J Chem Phys 82(1):299–310
53. Hay P, Wadt W (1985) Ab initio effective core potentials for molecular calculations. Potentials for main group elements sodium to bismuth. J Chem Phys 82:284–298
54. Hay PJ, Wadt WR (1985) Ab initio effective core potentials for molecular calculations. Potentials for the transition metal atoms Sc to Hg. J Chem Phys 82(1):270–283